Electronic structure of staging dislocations, electron scattering states, and the residual resistance of graphite intercalation compounds

Sergio E. Ulloa* and George Kirczenow
Department of Physics, Simon Fraser University, Burnaby, British Columbia, Canada V5A 1S6
(Received 14 July 1986)

A theoretical analysis of the electronic properties of staging domain walls in graphite intercalation compounds is presented. We show that the charge carriers in these materials have a vanishingly small probability of being backscattered from any smooth impurity or defect potential treated within $\mathbf{k}\cdot\mathbf{p}$ theory. These unique scattering properties of electrons in the conical bands of graphite are a consequence of the layer lattice symmetry, and result in anomalous tunneling through staging dislocations. The contribution to the residual resistance by the staging domain walls is calculated via the solution of the Boltzmann equation for several model wall arrangements in stage-2 compounds. A Thomas-Fermi description of the inhomogeneous charge distribution across a wall and corresponding self-consistent potentials is used in the evaluation of the scattering rate functions. The theory predicts an unusually low residual resistivity for an array of elongated domains with parallel domain walls, as a consequence of the anomalous tunneling. On the other hand, large residual resistivity values are obtained for typical domain and wall sizes in the case of a random arrangement of walls. We propose that accurate residual resistivity measurements be used as a macroscopic probe of the Daumas-Hérold domain structure, of the unusual transport properties, and of the kinetics of intercalation in these compounds. Other experimental implications of the theory are also discussed.

I. INTRODUCTION

The electronic properties of graphite intercalation compounds have attracted a great deal of attention in the study of these materials, and especially so in recent years.[1,2] Much effort has been devoted to work on the in-plane electrical conductivity since the physical understanding of the large values achieved in some compounds offers an interesting challenge as well as very attractive practical possibilities. However, the detailed scattering properties of the charge carriers in these compounds have not received the same attention. In this paper we present an analysis of the in-plane scattering properties of electrons and holes in graphite intercalation compounds. We show that the scattering has very unusual characteristics, which include a weak backscattering probability from any smoothly-varying impurity or defect potential in these systems.

On the other hand, due to a large range of very elegant experiments,[1-3] it is now widely believed that the Daumas-Hérold (DH) model of staging[4,5] is generally a good description of the arrangement of the intercalate guest in intercalation compounds. This model, in which the intercalate units are found in all of the galleries of the host forming microscopic well-staged domains (see Fig. 1), plays an important role in the kinetics of intercalation. The consequences of DH domains in the thermodynamics and kinetics of intercalation have just recently started to be considered quantitatively.[6-8] However, their effect on the electronic properties of these compounds has not received much attention.[9] We present here a microscopic calculation of the electronic scattering by these extended staging imperfections, and the corresponding contribution to the in-plane residual resistivity of stage-2 graphite intercalation compounds.

The formation of graphite intercalation compounds is always accompanied by a transfer of electrons to or from the graphite host.[1,2] Experiments and theory suggest that this excess charge is homogeneously distributed within the graphite layers.[10,11] It is this transferred charge, together with the large in-plane mobility,[12] which is responsible for the large conductivity enhancement observed after intercalation. However, we find that the presence of DH domain walls (regions void of intercalate between adjacent domains, see Fig. 1) greatly affects the level of local charge transfer to the graphite layers and results in inhomogeneous potentials. These potentials are strong for typical wall widths and cause scattering of electrons, producing a contribution to the residual resistivity. Also, the varying effective charge transfer across a staging dislocation should locally affect the changes in carbon bond length observed in the graphite host after intercalation.[13,14]

The resulting resistivity values due to the staging dislocations reflect the unique scattering properties of the carriers. In the case of an irregular array of domains (a likely configuration in typical samples), we obtain large resi-

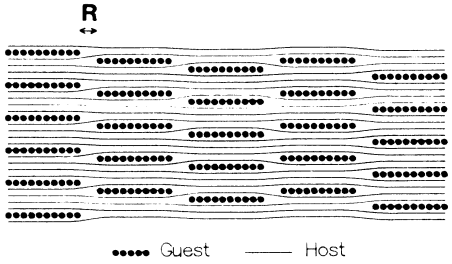

FIG. 1. Schematic Daumas-Hérold structure in a stage-4 compound.

dual resistivities, comparable with experimental values, suggesting that this is the most important scattering mechanism in high quality samples at low temperatures. If confirmed by detailed experimental measurements of domain sizes and conductivities, this suggestion together with the present theoretical results should enable the use of residual resistivity measurements as a quantitative *bulk* probe of the Daumas-Hérold structure, which must currently be studied using much more demanding experimental techniques.[1-3] These calculations could also explain the observed large differences in residual resistivity measurements in different samples of the same compound, since change in sample preparation can give rise to totally different domain structures in the final product (as shown in recent computer simulations of intercalation).[7] The residual resistivity also presents a strong dependence on the DH wall width which could possibly be used to monitor the kinetics of intercalation, an area of growing interest.[1-3,6-8,15] Furthermore, we predict that the residual resistivity in stage-2 systems with random domain-wall configurations should *increase*, although only slightly, with increasing charge transfer per carbon atom (other parameters fixed). This is in contrast with naive intuitive ideas of intercalation, and results from the strong inhomogeneity of the scattering potential. The theory also predicts that in the case of a sample with long and parallel intercalate domains, the weak electronic backscattering would produce an *in-plane* anisotropy of the residual resistivity. The residual resistivity in this case would achieve vanishingly small values in the direction perpendicular to the domains, possibly even having practical applications. These theoretical observations strongly suggest that further detailed and systematic measurements of the residual resistivity,[16] together with careful observations of domain size and shape on the *same* samples should yield very interesting results.

The remainder of this work is organized as follows.[17] In Sec. II we present a $\mathbf{k}\cdot\mathbf{p}$ formalism which can be used to treat the intralayer scattering of electrons by a defect potential in these compounds.[11] We also discuss the unusual scattering properties described by the resulting "effective-mass" equations. In Sec. III we calculate the self-consistent potentials and transferred charge profiles across DH walls using a Thomas-Fermi formulation. This section also contains the resulting transmission coefficients for the conduction carriers across those potentials In Sec. IV we present the solution to the Boltzmann equation for several DH wall distributions, and calculate the corresponding contribution to the residual resistivity of such arrangements. We also present results for the residual resistivity of specific compounds, and compare them with experimental values. This makes it possible to estimate domain sizes in the samples where the measurements were taken. Finally, in Sec. VI we discuss some of the important experimental implications of the electronic structure of DH walls.

II. EFFECTIVE-MASS EQUATION

In this section we present the equivalent of the effective-mass equation satisfied by the conduction electrons or holes in graphite intercalation compounds.[11] The formalism considers a model of electronic bands in two-dimensional graphitic layers. The two-dimensional character of the bands has been previously used with success in the analysis of experiments that probe states near the Fermi level, particularly in the case of acceptor guest compounds.[18-20] This approach provides a clear physical insight into the scattering situation and avoids the computational complexity of *ab initio* calculations.

It is well known that due to lattice symmetry the valence and conduction bands in two-dimensional graphite are degenerate at the corners of the hexagonal Brillouin zone (point P).[1,2] It is through this point that the Fermi level passes in the absence of charge transfer to the graphite layers, resulting in a zero-gap semiconductor. In consequence, the treatment of the conduction charges under moderate charge transfer which populates only these degenerate bands, requires the simultaneous consideration of the two Bloch states at point P in the $\mathbf{k}\cdot\mathbf{p}$ formalism.[21] If we denote these orthonormal states by $\phi_1(\mathbf{r})$ and $\phi_2(\mathbf{r})$, we can make the following Ansatz for the solution of the Schrödinger equation in the vicinity of point P,

$$\psi(\mathbf{r})=\sum_j \int d\mathbf{k}\, f_j(\mathbf{k}) e^{i\mathbf{k}\cdot\mathbf{r}}\phi_j(\mathbf{r}) , \tag{2.1}$$

where $j=1,2$; the two-dimensional vectors $\mathbf{k}$ and $\mathbf{r}$ are defined in the graphite plane (in the case of a curved graphite layer such as occurs at a DH wall, $\mathbf{r}$ represents curvilinear coordinates locating points in the nonplanar layer); and $\mathbf{k}$ is measured from point P. Inserting Eq. (2.1) into the Schrödinger equation and keeping up to linear terms in $\mathbf{k}$, one obtains

$$Ef_j(\mathbf{k})=(\hbar/m)\sum_i \mathbf{k}\cdot\mathbf{p}_{ji} f_i(\mathbf{k})+\int d\mathbf{k}' f_j(\mathbf{k}')\tilde{U}(\mathbf{k}-\mathbf{k}') , \tag{2.2}$$

where

$$\mathbf{p}_{ji}=\int d\mathbf{r}\phi_j^*(\mathbf{r})(-i\hbar\nabla)\phi_i(\mathbf{r}) \tag{2.3}$$

are the matrix elements of the momentum operator in this basis, E is the energy measured from the degenerate point P, and

$$\tilde{U}(\mathbf{q})=\int d\mathbf{r}\, e^{-i\mathbf{q}\cdot\mathbf{r}}U(\mathbf{r}) , \tag{2.4}$$

with $U(\mathbf{r})$ being the defect or impurity scattering potential. Notice that in writing Eq. (2.2) we have made the standard effective-mass approximation of a slowly-varying potential $U(\mathbf{r})$, which will only couple small $\mathbf{k}$ vectors, ignoring intervalley scattering (in graphite there are two portions of the Fermi surface at different corners of the Brillouin zone), as well as interband transitions.[21]

The symmetry of the hexagonal graphite lattice can be used to show that[22]

$$\mathbf{p}_{11}=\mathbf{p}_{22}=0,\quad \mathbf{p}_{12}=\mathbf{p}_{21}^*=mv_F(\hat{\mathbf{x}}-i\hat{\mathbf{y}}) , \tag{2.5}$$

where $\hat{\mathbf{x}}$ and $\hat{\mathbf{y}}$ are the Cartesian unit vectors, and $v_F=9.71\times10^7$ cm/sec is a real constant whose value is determined below from the band dispersion in the absence of the defect potential U. Using Eq. (2.5) one can write the Fourier transform of Eq. (2.2) as

$$[E-U(\mathbf{r})]F_j(\mathbf{r})=-i\hbar v_F\sum_{j'}\hat{D}_{jj'}F_{j'}(\mathbf{r}) , \tag{2.6}$$

where $\hat{D}$ is a first-order differential matrix operator with elements,

$$\hat{D}_{11}=\hat{D}_{22}=0\ ,$$
$$\hat{D}_{12}=\hat{D}_{21}^{*}=\partial/\partial x+i\partial/\partial y\ , \tag{2.7}$$

and the real-space envelope functions F are given by

$$F_j(\mathbf{r})=\int d\mathbf{k} f_j(\mathbf{k})e^{i\mathbf{k}\cdot\mathbf{r}}\ , \tag{2.8}$$

which allow Eq. (2.1) to be written as

$$\psi(\mathbf{r})=\sum_j F_j(\mathbf{r})\phi_j(\mathbf{r})\ . \tag{2.9}$$

In the absence of a disturbance potential ($U=0$), one can easily diagonalize Eq. (2.6) and reproduce the well-known linear-band dispersion relation of two-dimensional graphite[1,2,18,22]

$$\varepsilon(\mathbf{k})=\pm\hbar v_F k\ , \tag{2.10}$$

where $k=|\mathbf{k}|$, and the $(+)$ or $(-)$ sign refers to the conduction or valence band, respectively. The corresponding unperturbed wave functions are

$$\phi_{\mathbf{k}}^{\pm}(\mathbf{r})=e^{i\mathbf{k}\cdot\mathbf{r}}[\phi_1(\mathbf{r})\pm\phi_2(\mathbf{r})e^{i\theta_{\mathbf{k}}}]/\sqrt{2}\ , \tag{2.11}$$

where

$$\theta_{\mathbf{k}}=\tan^{-1}(k_y/k_x)\ . \tag{2.12}$$

Expression (2.6) above plays the role of the effective-mass equation for the electrons in graphite intercalation compounds. The peculiar first-order form, and attendant wave functions and linear-band dispersion relation in the unperturbed case [Eqs. (2.10) and (2.11)], are a consequence of the symmetry properties of the graphitic-layer lattice which yield a nonvanishing matrix element $\mathbf{p}_{12}$, Eq. (2.5). In the more common situation, all of the intraband matrix elements of $\mathbf{p}$ vanish at a band extremum, and the interband quadratic terms $[O(k^2)]$ provide the first nonvanishing contribution to the $\mathbf{k}\cdot\mathbf{p}$ equation. In this latter case one recovers the free-electron-like second-order differential equation, where the bare electronic mass is replaced by the effective mass.[21]

These unique characteristics of Eq. (2.6) also result in very unusual scattering properties for the electrons and holes in these compounds. Let us consider the scattering by a localized potential $U(\mathbf{r})$ which varies slowly enough for Eq. (2.6) to be valid. Examples of such a potential are those produced by an interstitial[11] or by a substitutional impurity like B or N in graphite.[23] The *asymptotic* wave functions for a scattering particle in such a case will be formed by linear combinations of functions $\phi_{\mathbf{k}}$ of Eq. (2.11). An indication of the anomalous character of the scattering can be seen in the vanishing of the matrix element joining any two asymptotic states with *opposite* wave vector: In general, we can write the matrix element of U between states $\phi_{\mathbf{k}}$ and $\phi_{\mathbf{k}'}$ in terms of its Fourier transform as,

$$\langle\phi_{\mathbf{k}}|U|\phi_{\mathbf{k}'}\rangle=\tilde{U}(\mathbf{k}'-\mathbf{k})\{1+\exp[i(\theta_{\mathbf{k}}-\theta_{\mathbf{k}'})]\}/2\ , \tag{2.13}$$

where we have assumed $U(\mathbf{r})$ to be spatially smooth and we have used the orthonormality of ϕ_1 and ϕ_2. It is clear that for any $\mathbf{k}'$ antiparallel to $\mathbf{k}$ (i.e., $\theta_{\mathbf{k}'}=\theta_{\mathbf{k}}+\pi$, with $k'\neq k$ in general), Eq. (2.13) *vanishes*. This implies that a slowly-varying potential is not able to backscatter conduction electrons or holes in these compounds, even when $\tilde{U}(\mathbf{k}'-\mathbf{k})\neq 0$. This is purely a result of the symmetry properties of the graphite layers which result in Eqs. (2.5) and (2.6), and the corresponding wave functions in Eq. (2.11). It would be very interesting to see if other materials with similar dispersion relation (or lattice symmetry) would also exhibit this electron scattering behavior.

In the case of a linear defect, with potential varying only in a given direction x (like in the case of a DH wall, see Sec. III), the scattering becomes a one-dimensional problem since the potential will not affect the motion in the orthogonal y direction. Therefore, by an argument similar to the one above, the matrix element $\langle\phi_{k_x,k_y}|U(x)|\phi_{-k_x',k_y}\rangle$ must not vanish for at least some values of k_x', if the potential is to be able to scatter a charge carrier. This matrix element can be expressed in terms of the k components of the potential as

$$\langle\phi_{k_x,k_y}|U(x)|\phi_{-k_x',k_y}\rangle$$
$$=\tilde{U}(k_x'+k_x)\{kq-k_xk_x'+k_y\times[k_y-i(k_x+k_x')]\}/(2kq)\ , \tag{2.14}$$

with $q=[(k_x')^2+k_y^2]^{1/2}$ and $k=(k_x^2+k_y^2)^{1/2}$. Notice that for *any* $-k_x'$ (with opposite sign to k_x), and for normal incidence to the linear defect ($k_y=0$), this matrix element *vanishes identically* and the defect cannot scatter. As a consequence, the tunneling coefficient for such a potential will approach a value of unity for near-normal incidence to the linear defect, *irrespective* of the magnitude of $\tilde{U}$. This is indeed a very surprising result if one compares it with the results for a parabolic band: From elementary considerations in the quantum mechanics of a free-electron-like particle scattered from a finite potential, the tunneling coefficient is not unity and decreases for increasing potential strength.[24]

The weak backscattering property of the electronic wave functions described by Eq. (2.6) can be shown to persist even after the inclusion of the quadratic interband terms $[O(k^2)]$ neglected there. This underlines further the role of the lattice symmetry in providing such unusual scattering properties for arbitrary smoothly-varying potentials.

The very surprising result of near-perfect transmission through a barrier will be explicitly verified in Sec. III for the particular case of the DH wall potential obtained in a Thomas-Fermi approximation. However, the discussion in the present section shows the qualitative anomalies of the electronic scattering properties in these materials to be a *general* property, valid for any smooth potential, and solely derived from the graphite lattice symmetry. On the other hand, the possibility of carefully controlled synthesis of samples having certain special DH domain structures provides a natural vehicle for the experimental verification of these unusual scattering properties through the measurement of the residual resistivity of these materials. This will be further discussed in Sec. IV.

III. DOMAIN-WALL POTENTIALS

To first approximation, the main effect of the intercalation process is to populate the graphitic conical bands, shifting the Fermi level. This shift will be upwards in the case of donor guests, and downwards for acceptors. As discussed in the Introduction, the transferred charge is believed to be distributed homogeneously throughout the graphite layer to a good approximation.[10,11] However, across a DH wall the in-plane electron (or hole) distribution will be inhomogeneous, being greatly reduced near the center of the dislocation, as shown in this section. Here we calculate the self-consistent potentials and transferred charge profiles in a DH wall using a Thomas-Fermi formulation. This approach has been found adequate for the description of charge distributions in these compounds,[25,26] and should give at least a qualitative picture of the distribution across the DH dislocations.

One can derive the Thomas-Fermi equations of interest starting from the total energy E_T of a configuration of well-formed stage-2 domains across a DH wall,[27]

$$E_T/(NlI_c)=\tfrac{1}{2}\int dx\, V(x)\{n_i(x)-n(x)\} + \int dx\, t[n(x)]n(x)\ , \tag{3.1}$$

where we have chosen x to be the coordinate across the wall of thickness R, and length l ($\gg R$) in the perpendicular y direction. n_i and n are the intercalate-ion and carrier density, respectively; I_c is the stage period (in the c-axis direction), and N is the total number of intercalate layers. The first term in (3.1) represents the electrostatic energy, where the potential energy $V(x)$ satisfies Poisson's equation,

$$d^2V/dx^2=4\pi e^2[n(x)-n_i(x)]/\epsilon\ , \tag{3.2}$$

and $\epsilon=2.4$ is the *in-plane* static dielectric constant which includes the screening by the nonconduction electrons.[28,29]

The second term in (3.1) considers the kinetic band energy of the charge. For the conical bands described by Eq. (2.10) one can calculate the total kinetic energy per electron as

$$t[n]=\tfrac{2}{3}\beta n^{1/2}\ , \tag{3.3}$$

where $\beta=\hbar v_F(\pi c_0)^{1/2}$, and $c_o=3.35$ Å is the interlayer separation in graphite.

Minimization of (3.1) with respect to $n(x)$ yields the relation between the potential and charge profile,

$$V(x)=\beta n^{1/2}(x)-\mu\ , \tag{3.4}$$

which substituted in (3.2) gives the self-consistent equation for the potential

$$d^2\chi(\zeta)/d\zeta^2=\chi^2(\zeta)-\tilde{n}_i(\zeta)\ , \tag{3.5}$$

where $\chi=1+\tilde{V}$, $\tilde{V}=V/\mu$, $\tilde{n}_i=I_c n_i/n_0$, $\zeta=\lambda x$, and

$$\lambda^2=4\pi e^2(n_0/I_c)^{1/2}/(\epsilon\beta)\ . \tag{3.6}$$

In these expressions, n_0 and $\mu=\beta(n_0/I_c)^{1/2}$ are, respectively, the in-plane carrier density and Fermi level in the regions far from the DH wall. The carrier density is related to the charge-transfer coefficient f by

$$n_0=4f/(ra_0^2\sqrt{3})\ , \tag{3.7}$$

where $a_0=2.46$ Å is the in-plane graphite lattice constant and r is the number of carbon atoms per intercalate, in a compound of guest X and formula C_rX. Notice that there is no distinction between donor or acceptor guests in this treatment (i.e., the sign of f), since the conical valence and conduction bands described by Eq. (2.10) are totally symmetric. We are then only interested in the magnitude of the charge-transfer coefficient f.

The dimensionless equation (3.5) is solved numerically for the potential and corresponding charge profile in the case of a continuum intercalate-ion density on both sides of a DH wall of width R,

$$\tilde{n}_i(\zeta)=\Theta(\zeta-\tilde{R}/2)+\Theta(-\zeta-\tilde{R}/2)\ , \tag{3.8}$$

where $\tilde{R}=\lambda R$, and Θ is the usual unit step function. The corresponding asymptotic boundary conditions on χ are: $\chi\to 1$, and $d\chi/d\zeta\to 0$ for $\zeta\to\pm\infty$.

Figure 2 shows examples of the *universal* curves obtained for the normalized potential energy $\tilde{V}=V/\mu$, and charge profile $\tilde{n}=I_c n/n_0$. As expected, the charge transferred to the graphite layers is greatly reduced near the center of the DH wall, especially for larger wall widths, although the effect is also very strong for walls of typical widths in thermodynamic equilibrium ($R\simeq 10$ Å, $\tilde{R}\simeq 3$–4 in these units).[8] Correspondingly, the resulting self-consistent potential V reaches a maximum value in the middle of the wall nearly equal to μ. It is this potential which will produce the in-plane scattering of conduction electrons or holes when they approach the DH wall region.

In addition to its influence on electronic transport, the inhomogeneous charge transfer across a DH wall should affect the carbon-carbon bond length in this region. it is now well established that the charge transfer to the graphite layers which occurs with intercalation affects the carbon nearest-neighbor distances.[13,14] It is therefore possible that detailed measurements of the graphite layer bond lengths would show greater dispersion in samples with a large number of DH walls than in more uniformly intercalated samples. Together with elastic effects, this should influence the value of f extracted from bond-length measurements,[14] and should be considered in interpreting the results.

Let us now calculate the transmission probability through a DH wall potential like those depicted in Fig. 2. Since V vanishes asymptotically on either side of the DH wall, the solution of Eq. (2.6), with V as the potential U, will be a linear combination of functions $\phi_{\mathbf{k}}$ of Eq. (2.11) for points far from the wall. All of the arguments leading to the matrix element of Eq. (2.14) and its corresponding vanishing for normal incidence to the wall will be valid here. Therefore, we expect a large normal-incidence tunneling coefficient for these wall potentials, as it is explicitly verified below by an essentially exact numerical solution of Eq. (2.6).

The Appendix shows the detailed procedure followed to obtain the tunneling coefficient T through a DH wall. This is calculated for the conduction carriers falling on a wall of width R at an arbitrary angle θ measured with

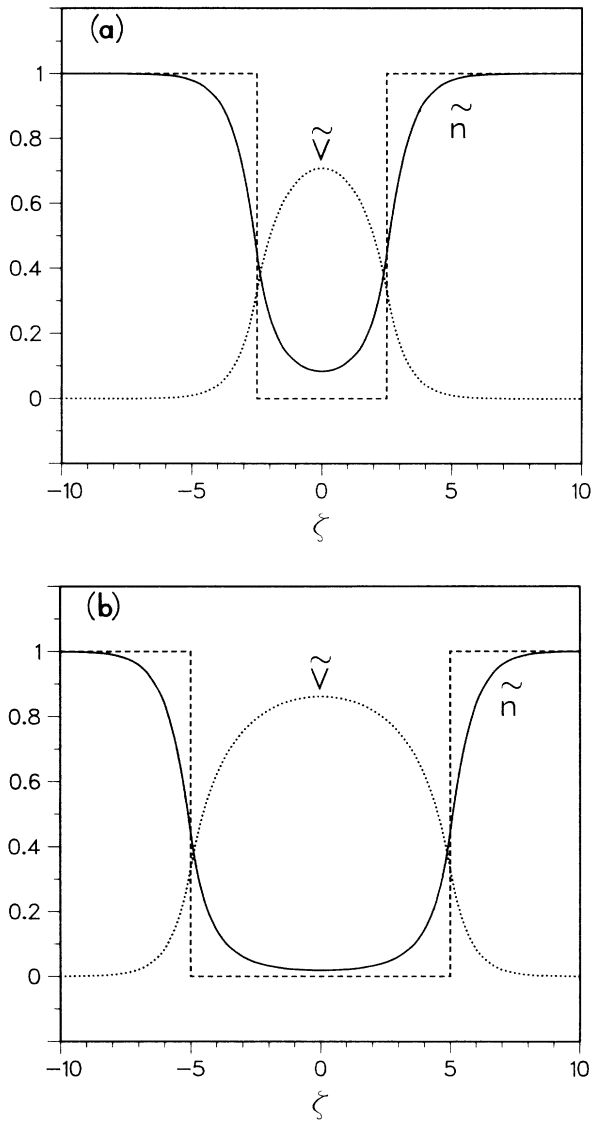

FIG. 2. Examples of universal curves for normalized electrostatic potential $\tilde{V}$ and charge profile $\tilde{n}$ across a DH domain wall. Dashed line indicates position of the intercalate-ion domains. (a) Wall width $\tilde{R}=5$. (b) $\tilde{R}=10$; notice increasing charge depletion near the middle, and corresponding larger maximum in $\tilde{V}$.

respect to the wall normal. Figure 3 shows $T(\theta)$ for several wall widths in the case of the stage-2 compound $C_{16}SbF_5$ ($I_c=11.76$ Å, $f=\frac{1}{4}$), as an example of typical results. As expected from the general arguments of Sec. II, the tunneling probability approaches a value of 1 for electrons falling at near-normal incidence to the wall, *irrespective* of the wall width R. Notice also in Fig. 3 that the range for which $T\simeq 1$ ("acceptance angle") decreases rapidly with increasing wall width R. Figure 4 shows the complementary plot of T versus R for several angles. One can see there that as long as the angle of incidence is nonzero, the tunneling probability decreases with increasing wall width, as intuitively expected.

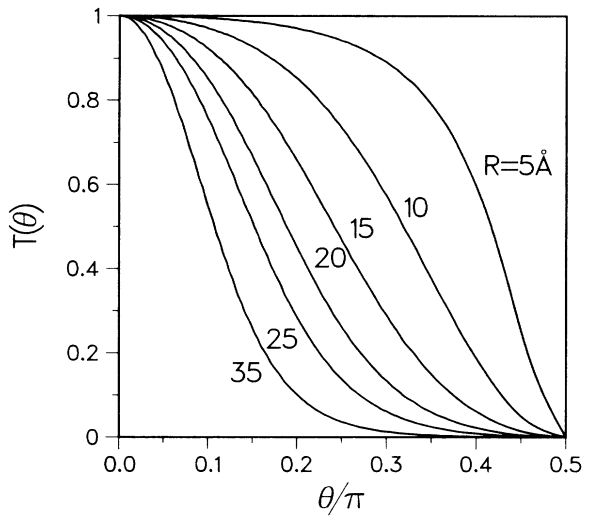

FIG. 3. Tunneling coefficient for conduction carriers T versus the angle of incidence to the wall θ, for several wall widths R, in the compound $C_{16}SbF_5$. Notice transparency of walls for near-normal incidence, and all values of R.

The near-perfect transparency of a DH wall for near-normal incidence is an explicit demonstration of the unusual scattering properties of the conduction charges in these compounds. This provides us with a physical mechanism for the possible experimental verification of the anomalous scattering and its exciting possibilities. This will be discussed further in the following section. There we also show that the limited acceptance angle results in a sizable overall scattering probability for electrons falling with random orientations to a wall of typical width ($\simeq$10 Å), resulting in large residual resistivity contributions from DH walls alone.

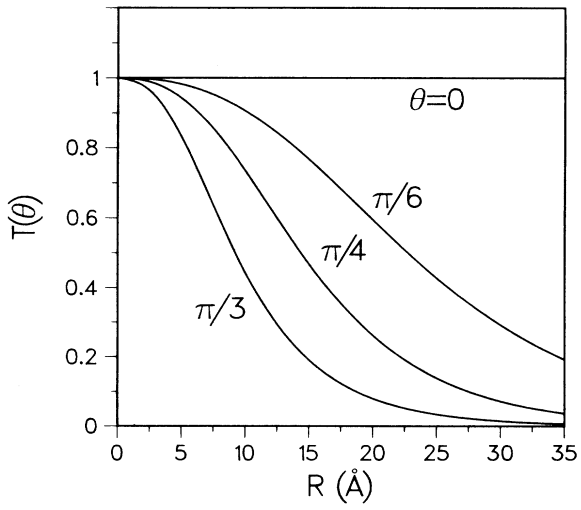

FIG. 4. T vs R for several incidence angles in $C_{16}SbF_5$.

IV. RESIDUAL RESISTIVITY

In order to find the contribution of the DH walls to the residual resistivity in these compounds we proceed to solve the Boltzmann equation. Since the scattering properties of the electrons in these compounds are strongly dependent on the angle of incidence to the wall, as shown in the preceding section, we will find the resistivity for several geometrically distinct wall arrangements below: (a) parallel elongated walls with the electric field perpendicular to them; (b) randomly oriented walls; and (c) walls arranged with a relative 60° angle.

The Boltzmann equation for an extended system in the presence of only an electric field $\mathbf{E}$ has the form[30]

$$(-\partial f_{\mathbf{k}}^0/\partial\varepsilon_{\mathbf{k}})\mathbf{v}_{\mathbf{k}}\cdot e\mathbf{E}=(-\partial f_{\mathbf{k}}/\partial t)\,|_{\text{scatt}} = \int d\mathbf{k}'(s_{\mathbf{k}}-s_{\mathbf{k}'})Q(\mathbf{k},\mathbf{k}') , \quad (4.1)$$

where $\mathbf{v}_{\mathbf{k}}=\partial\varepsilon_{\mathbf{k}}/\hbar\partial\mathbf{k}$, and $Q(\mathbf{k},\mathbf{k}')$ is the scattering probability per unit time per unit volume of $\mathbf{k}$ space, which connects electronic states with wave vectors $\mathbf{k}$ and $\mathbf{k}'$. Here,

$$f_{\mathbf{k}}^0=f^0(\varepsilon_{\mathbf{k}})=(1+e^{\beta(\varepsilon_{\mathbf{k}}-\mu)})^{-1} \quad (4.2)$$

is the equilibrium Fermi distribution for the chemical potential μ and temperature $T=(k_B\beta)^{-1}$, where k_B is the Boltzmann constant, and the function $s_{\mathbf{k}}$ is the departure from the equilibrium distribution,

$$s_{\mathbf{k}}=f_{\mathbf{k}}-f_{\mathbf{k}}^0 . \quad (4.3)$$

We will be solving Eq. (4.1) for each of the scattering probability functions $Q(\mathbf{k},\mathbf{k}')$ which depend on the distribution of walls in a sample of stage 2, and use this solution function $s_{\mathbf{k}}$ to calculate the electrical current density $\mathbf{J}$, with

$$\mathbf{J}=(4e/I_c)\sum_{\mathbf{k}}\mathbf{v}_{\mathbf{k}}s_{\mathbf{k}} , \quad (4.4)$$

where the factor of 4 includes the spin and valley degeneracies of the electronic states in graphite.[31]

A. Parallel walls

In this subsection we assume that most of the DH domains in the sample are elongated and the domain walls are randomly placed but aligned nearly parallel to each other, with the electric field perpendicular to them, $\mathbf{E}=\hat{x}E$. In this case the scattering probability that appears in Eq. (4.1) is given by

$$Q(\mathbf{k},\mathbf{k}')=(1/k)P_{\mathbf{k}}(\alpha)\delta(k-k')\delta(\alpha'+\alpha-\pi) , \quad (4.5)$$

where the delta factors explicitly show the elastic character of the scattering and the fact that the wave-vector component normal to the field (k_y) is conserved, changing the angle of incidence α into $\pi-\alpha$ after the scattering (α is measured with respect to the field direction). The factor $P_{\mathbf{k}}$ is the scattering rate for electrons moving in a region of domain walls separated by an average distance L, and is given by

$$P_{\mathbf{k}}(\alpha)=v_{\mathbf{k}}\cos\alpha\,[1-T(\alpha)]/L , \quad (4.6)$$

where $T(\alpha)$ is the transmission coefficient calculated in Sec. III. The $\cos\alpha$ factor takes into consideration the effective scattering cross section of the DH wall, which is assumed to be proportional to the wall length projected normally to the direction of incidence.

Substituting (4.5) into (4.1), one immediately obtains

$$s_{k,\alpha}-s_{k,\pi-\alpha}=(-\partial f_{\mathbf{k}}^0/\partial\varepsilon_{\mathbf{k}})eEv_{\mathbf{k}}\cos\alpha/P_{\mathbf{k}}(\alpha) , \quad (4.7)$$

where $s_{\mathbf{k}}=s_{\mathbf{k},\alpha}=s_{k_x,k_y}$. This difference of s functions can be used directly to calculate the corresponding current density without having an expression for $s_{k,\alpha}$ itself. Since $\mathbf{v}_{\mathbf{k}}=\mathbf{k}v_F/k$ for this case of conical bands, and $(k,\pi-\alpha)=(-k_x,k_y)$, we can write,

$$J_x=(4e/I_c)\sum_{k_y}\sum_{k_x}v_F(k_x/k)s_{k_x,k_y} =(4ev_F/I_c)\sum_{k_y}\sum_{k_x>0}(k_x/k)(s_{k_x,k_y}-s_{-k_x,k_y}) . \quad (4.8)$$

Using (4.7), replacing the sums by integrations in the usual fashion, and taking the zero-temperature limit, we obtain the following expression for the *residual resistivity* produced by the parallel DH walls (pw) in a sample,

$$\rho_{\text{pw}}=\hbar k_F I_c/(e^2 n_0 v_F\tau_{\text{pw}}) , \quad (4.9)$$

where $k_F=(\pi n_0)^{1/2}$, n_0 is defined in Eq. (3.7), and

$$\tau_{\text{pw}}=(2L/\pi v_F)\int_0^{\pi/2}d\alpha\cos\alpha[1-T(\alpha)]^{-1} . \quad (4.10)$$

Using these expressions and the tunneling coefficient calculated as in Sec. III, one can find the residual resistivity ρ_{pw}. We find that ρ_{pw} *vanishes* for all possible wall widths since the scattering time τ_{pw} diverges for *any* value of the wall width R. This is a consequence of the near-perfect transmission of the wall at small angles, discussed in preceding sections, which produce a divergent integrand in Eq. (4.10) for $\alpha\simeq 0$. Therefore, in a sample with mostly parallel domain walls, the DH-wall contribution to the residual resistivity will be anomalously small in the direction perpendicular to the walls. Furthermore, one would expect very anisotropic behavior in the *in-plane* residual resistivity for this kind of wall configuration in a sample. Experimental verification of this prediction would provide valuable insight into the very interesting and unique scattering properties of the charge carriers in these materials.

B. Random distribution of walls

We now consider the case of randomly distributed and oriented walls in a system. This is probably the model distribution that best reflects the situation in most experimental samples, especially those where restacking of the host does not occur (see Sec. IV C below for a discussion of the restacked case). In this configuration, the scattering function is

$$Q(\mathbf{k},\mathbf{k}')=(1/k)\tilde{Q}_{\mathbf{k}}(\Phi)\delta(k-k') , \quad (4.11)$$

where the scattering angle is $\Phi=\alpha-\alpha'$, and the scattering rate function for DH walls $\tilde{Q}_{\mathbf{k}}$ is given by

$$\tilde{Q}_{\mathbf{k}}(\Phi)=v_{\mathbf{k}}\sin(\Phi/2)\{1-T[(\pi-\Phi)/2]\}\gamma/L , \quad (4.12)$$

where $T(\alpha)$ is the transmission coefficient, and $\gamma \simeq 3$ is a geometrical factor. This factor γ relates the concentration of DH walls to the average size L of the domains and depends on the shape of the intercalate islands. Notice that Eq. (4.11) contains only one delta function describing elastic scattering at any value of the incidence angle α, measured with respect to the direction of the electric field. This function Q thus describes scattering from domain walls having all orientations.

Since Q in Eq. (4.11) only depends on the relative scattering angle Φ, one can prove that the solution to the Boltzmann equation can be written as

$$s_{\mathbf{k}} = (-\partial f_{\mathbf{k}}^0 / \partial \varepsilon_{\mathbf{k}}) e \mathbf{v}_{\mathbf{k}} \cdot \mathbf{E} \tau_1(k) , \tag{4.13}$$

where

$$1/\tau_1(k) = \int d\mathbf{k}' (1 - \cos\Phi) Q(\mathbf{k}, \mathbf{k}') . \tag{4.14}$$

This is the two-dimensional analog of the well-known spherically-symmetric elastic scattering which also produces a similar weighting factor of $(1 - \cos\Phi)$ in the scattering time.[30]

Correspondingly, the appropriate current density can be calculated, Eq. (4.4), and the residual resistivity one obtains in this case is given by

$$\rho_{\text{random}} = \hbar k_F I_c / [e^2 n_0 v_F \tau_1(k_F)] , \tag{4.15}$$

which is a similar expression to that of Eq. (4.9), but with τ_{pw} substituted by $\tau_1(k_F)$,

$$1/\tau_1(k_F) = \left[\frac{1}{2\pi} \right] \int_0^{\pi} d\Phi [1 - \cos\Phi] \tilde{Q}_{k_F}(\Phi) . \tag{4.16}$$

Notice from (4.16) and (4.12) that τ_1 is proportional to the average domain size L. Therefore, the product $L\rho_{\text{random}}$ will only depend on the domain wall width R for a given compound, i.e., for given values of the charge-transfer coefficient f, the component ratio r, and the c-axis period I_c. Figure 5 shows curves of $L\rho_{\text{random}}$ versus R for several stage-2 compounds [KC_{24} ($I_c = 8.75$ Å, $f = 1$), $C_{16}AsF_5$ ($I_c = 11.3$ Å, $f = 0.4$), and $C_{16}FeCl_3$ ($I_c = 12.8$ Å, $f = \frac{1}{4}$)]. It is clear that the residual resistivity due to the DH domain walls increases rather rapidly with wall width, approximately doubling the value of the resistivity every 5 Å. This is very different from what was found in the case of parallel walls, where the width of the wall did not affect the vanishing of the resistivity. The nonvanishing value of ρ_{random} comes from the small acceptance angle displayed in Fig. 3, as well as the fact that the wall distribution is randomly oriented. The large sensitivity of ρ_{random} to the wall width could probably be used as a probe in monitoring the intercalation kinetics, at least over the range of stability of a given stage, where small changes in the chemical potential produce different values for the *equilibrium* wall width.[8] It is also possible that this R dependence would result in an important contribution to the variation of the resistivity with pressure which has been observed in recent experiments.[1,32]

Results for calculated thermodynamic equilibrium values of the DH wall width R ($\simeq$8–10 Å),[8] and experimentally observed domain sizes L ($\simeq$100–10 000 Å)[1–3] yield large values of the residual resistivity. For example,

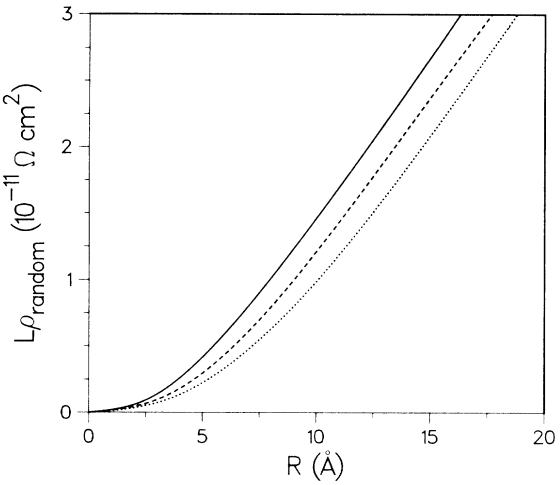

FIG. 5. Wall-width dependence of $L\rho_{\text{random}}$ for characteristic stage-2 compounds: KC_{24} denoted by solid line, $C_{16}AsF_5$ denoted by dashed line, and $C_{16}FeCl_3$ denoted by dotted line.

from Fig. 5 and the above ranges of R and L one obtains a range of possible values for $\rho_{\text{random}} \simeq 0.1$–10 $\mu\Omega$ cm, which is certainly comparable to typical experimental values of the in-plane residual resistivity $\rho_{\text{exp}} \simeq 0.5$ $\mu\Omega$ cm.[2,12,16,33,34] Therefore, it seems quite plausible that the DH domain-wall scattering mechanism provides the *dominant* contribution to the residual resistance in high-quality samples which have been made using single crystals of graphite. Furthermore, because of the large contribution of the DH walls to the residual in-plane resistance and its dependence on the domain size, we propose that measurements of this quantity could be used as a *bulk probe* of the Daumas-Hérold structure. This structure is presently studied using very demanding microscopic techniques[1–3] which would be complemented by the simpler resistivity measurements.

In order to illustrate this suggestion we show in Table I calculated values of $L\rho_{\text{random}}$ with the corresponding values of f and wall width R, for several stage-2 compounds for which experimental values of the in-plane residual resistivity exist in the literature.[2,12,16,33,34] The value of R chosen for the potassium guest (10 Å) is the equilibrium wall width derived from thermodynamic data, and the value for other guests is assumed to be 8 Å, in similitude to that derived for the bromine guest.[8] From these values of $L\rho_{\text{random}}$ we calculate the average DH domain size present in the samples where the experiments were performed, with the assumption that the observed resistances arise only from this scattering mechanism. This provides a *lower bound* L_{lb} on the average DH domain size, also shown in Table I. Accordingly, L_{lb} is 2 to 6 times larger in K-graphite than in the other compounds with the large-molecule acceptor guests. This qualitative trend in L_{lb} is indeed consistent with the experimentally observed values for L in different compounds,[1–3] and it is related to the different kinetic properties of the guest species.[1–3,8] For example, domain sizes of $\lesssim$2000 Å have been reported recently for the large-molecule guest $SbCl_5$,[35] while much larger domains are typically found in

TABLE I. In-plane residual resistivities for several stage-2 compounds.

Compound	f	I_c (Å)	R (Å)	$L\rho_{\text{random}}$ (10^{-11} Ω cm^2)	ρ_{exp} ($\mu\Omega$ cm)	L_{lb} (10^3 Å)
KC_{24}	1	8.75	10[a]	1.5	0.25[b]	6.0
$C_{16}SbF_5$	0.25	11.76	8	0.71	0.39[c]	1.8
$C_{16}AsF_5$	0.4	11.3	8	0.79	0.50[d]	1.6
$C_{16}HNO_3$	0.4	11.14	8	0.87	0.30[c]	2.9
$C_{17}OsF_6$	1	11.47	8	1.03	0.95[e]	1.1
$C_{20}TcF_6$	1	11.46	8	1.06	0.9[e]	1.2

[a]Reference 8.
[b]Reference 12.
[c]Reference 33.
[d]Reference 34.
[e]Reference 16.

the case of the heavy alkali guests ($\simeq$10 000 Å).[36] We believe that this promising comparison strongly suggests the possible utilization of the resistivity measurements as a macroscopic tool for the characterization of DH structures. This suggestion, however, requires further evaluation by careful measurements of domain size and residual resistance carried out on the same samples.[16]

The dependence of the resistivity on domain size also provides an explanation to the observed variations in residual resistivity for several samples of a given compound. It is very plausible, as shown in recent Monte Carlo simulations,[7] that differences in intercalation processes will produce very different domain structure and average intercalate island size, affecting the residual resistivity of the final product. This would further emphasize the need for systematic measurements of the residual resistivity in these compounds, keeping good control over factors that might affect the *microscopic* configuration of the samples.

As discussed above, the value of ρ_{random} depends also on the charge-transfer coefficient f and the c-axis period I_c. In Fig. 6 we show curves of $L\rho_{\text{random}}$ versus the charge-transfer *per carbon atom* f/r, for fixed I_c, and several wall widths R. Notice the slight *increase* of the resistivity with increasing charge transfer, which shows that the strong dependence of τ_1 on f/r unexpectedly *dominates* over the increasing surface carrier density n_0 [see Eq. (4.15)]. This indicates that the potential associated with the staging wall inhomogeneity becomes more pronounced with larger carrier density, and fixed wall width, producing stronger scattering. This is a result of the nonlinearity of the self-consistent carrier distribution across the wall.

In Fig. 7 we show the dependence of $L\rho_{\text{random}}$ on the c-axis period I_c for fixed values of f/r and R. This typical curve shows that the resistivity is nearly independent of the intercalate thickness with only a slight overall decrease for a large increment in I_c. Figures 6 and 7 together allow one to estimate the resistivity of any given compound (or more accurately, the product $L\rho_{\text{random}}$), with known values of f, I_c, and R. This estimate, together with the measured residual resistivity would allow the calculation of the average intercalate domain size in a sample as predicted by the present theory. This should facilitate

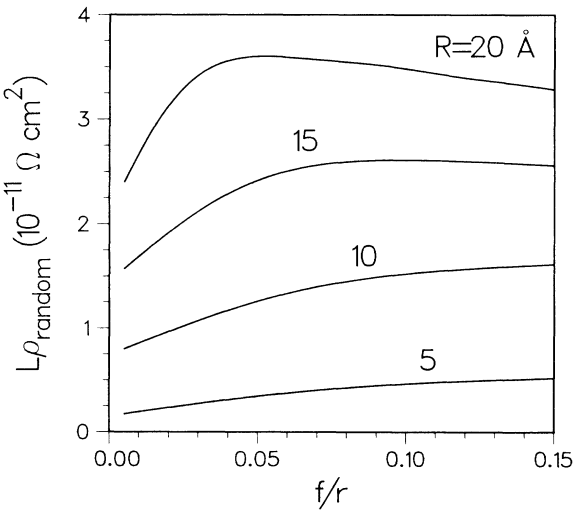

FIG. 6. $L\rho_{\text{random}}$ versus charge transfer per carbon atom f/r, for several wall widths R. Here, $I_c = 10$ Å. Notice increasing resistivity, especially for small f/r values.

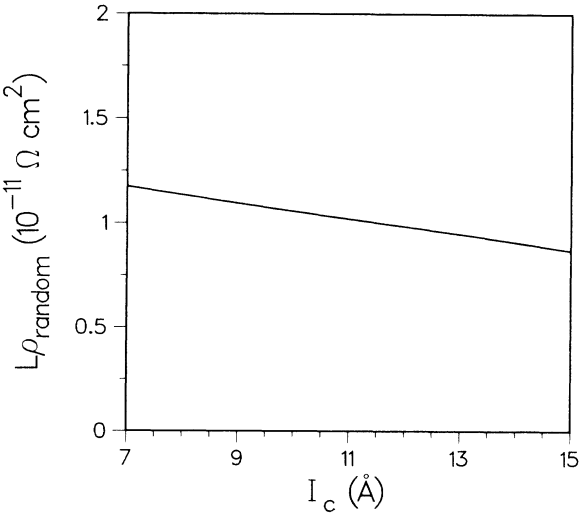

FIG. 7. Typical curve of residual resistivity versus intercalation compound period I_c, for constant $R = 10$ Å, and $f/r = 0.025$.

the direct comparison of experimental observations with the theory.

C. Domain walls with threefold orientational order

The substantial qualitative difference between the two wall arrangements discussed above suggests the study of another situation which we now address. This wall distribution is motivated by the physical situation which probably appears in the case of compounds that force the restacking of the host matrix (such as in K-, Li-, and Br_2-graphite).[1,2] The energetics of the local deformations at the DH walls in these compounds have been studied previously.[8] The energetics favor specific in-plane wall orientations, perpendicular to the lines joining carbon nearest neighbors in the graphite layer, in order to minimize in-plane shear. Since the carbon atoms in the graphite layer sit in a honeycomb array,[1,2] the DH walls in these restacked compounds will have mostly three in-plane orientations with a relative 60° angle. If the electric field is perpendicular to one of these three equivalent wall orientations, the scattering function is given by

$$Q(\mathbf{k},\mathbf{k}')=\left[\frac{1}{3k}\right]\delta(k-k') \times[P_{\mathbf{k}}(\alpha)\delta(\alpha'-\alpha_1)+P_{\mathbf{k}}(\pi/3-\alpha)\delta(\alpha'-\alpha_2) +P_{\mathbf{k}}(2\pi/3-\alpha)\delta(\alpha'-\alpha_3)] , \quad (4.17)$$

where $P_{\mathbf{k}}$ is the scattering rate function defined in Eq. (4.6), and the angles *after* scattering α_j are related to the angle of incidence α by

$$\alpha_1=\pi-\alpha,\ \alpha_2=5\pi/3-\alpha, \text{ and } \alpha_3=\pi/3-\alpha . \quad (4.18)$$

The delta function factors in (4.17) reflect the existence of the three possible wall orientations in this model configuration, and the fact that the scattering is assumed to be elastic and specular at each of the walls.

Unlike the previous cases, here we cannot solve the Boltzmann equation analytically, since the direct substitution of (4.17) into (4.1) would only yield a recurrencelike relation for the distribution function $s_{\mathbf{k}}$ at various angles. (This is known as a finite-difference equation.)

In order to obtain the solution to the *steady-state* equation which the distribution function $s_{\mathbf{k}}$ satisfies [Eq. (4.1)], we choose to solve the *time-dependent* equation which describes the relaxation of the function $s_{\mathbf{k}}(t)$ as[30]

$$\partial s_{\mathbf{k}}(t)/\partial t=(-\partial f^0_{\mathbf{k}}/\partial\varepsilon_{\mathbf{k}})\mathbf{v}_{\mathbf{k}}\cdot e\mathbf{E} - \int [s_{\mathbf{k}}(t)-s_{\mathbf{k}'}(t)]Q(\mathbf{k},\mathbf{k}')d\mathbf{k}' . \quad (4.19)$$

This clearly reduces to Eq. (4.1) in the steady-state situation, $\partial s_{\mathbf{k}}/\partial t=0$. We now assume that the time evolution only affects the angular dependence of the function s, since the scattering is elastic, so that we can define a function $h(\alpha,t)$ through the expression

$$s_{\mathbf{k}}(t)=(-\partial f^0_{\mathbf{k}}/\partial\varepsilon_{\mathbf{k}})3eLEh(\alpha,t) . \quad (4.20)$$

Here, h is a dimensionless function of angles and time which, with the use of (4.17) and (4.19), can be shown to obey the following equation,

$$\partial h(\alpha,\tilde{t})/\partial\tilde{t}=\cos\alpha-\sum_j[h(\alpha,\tilde{t})-h(c_j-\alpha,\tilde{t})]B(\alpha-d_j) , \quad (4.21)$$

where $\tilde{t}$ is a dimensionless time variable $\tilde{t}=v_FLt/3$; $B(\beta)=[1-T(\beta)]\cos\beta$, with T being the transmission coefficient through the wall; and the constants c_j and d_j are defined as $c_1=\pi$, $c_2=5\pi/3$, $c_3=\pi/3$, $d_1=0$, $d_2=\pi/3$, and $d_3=2\pi/3$.

Equation (4.21) is integrated numerically. We start from the equivalent solution in the case of a random-wall distribution: $h(\alpha,0)=\cos\alpha$, and iterate in time until we reach the steady-state solution ($\partial h/\partial\tilde{t}\simeq10^{-7}$ in our calculation). The solution $h_{\rm sol}(\alpha)$, which of course solves Eq. (4.1) by construction, is then used to calculate the resistivity via Eqs. (4.4) and (4.20), to obtain the by now familiar expression,

$$\rho_\Delta=\hbar k_F I_c/(n_0e^2v_F\tau_\Delta) , \quad (4.22)$$

with the scattering time given by

$$\tau_\Delta=(3L/\gamma v_F)\int_0^{2\pi}d\alpha\, h_{\rm sol}(\alpha)\cos\alpha . \quad (4.23)$$

In Fig. 8 we show curves of the function $h_{\rm sol}(\alpha)$ for several wall widths $\tilde{R}$ [$=\lambda R$, with λ defined by Eq. (3.6)], for the compound KC_{24} ($I_c=8.75$ Å, $f=1$, and $\lambda^{-1}=3.17$ Å). Notice that the steady-state angular distribution function presents the proper characteristics required by symmetry, such as periodicity modulo 2π, inversion symmetry with respect to the points $\pm\pi/2$, and reflection symmetry with respect to π, for all values of $\tilde{R}$. Notice also that the pronounced peak at $\alpha\simeq\pi/6$ for small $\tilde{R}$ changes over to a distribution with peaks at approximately $\pi/3$ intervals, for larger $\tilde{R}$. These latter angles are

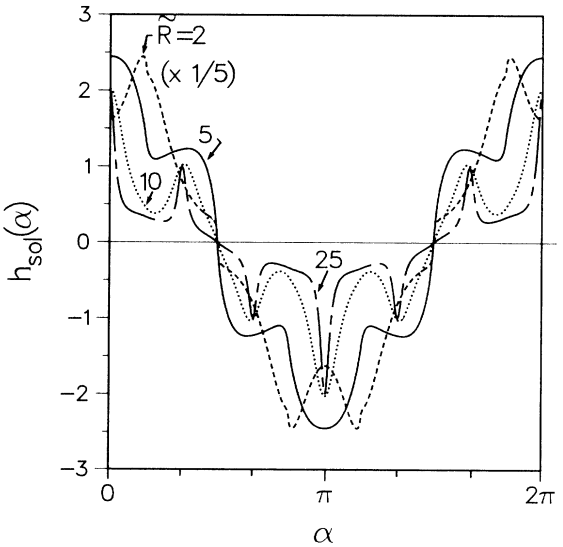

FIG. 8. Steady-state angular distribution function $h_{\rm sol}$ vs α, for several normalized wall widths $\tilde{R}$ in KC_{24}. Dashed curve for $\tilde{R}=2$ has been scaled *down* by a factor of 5. Notice peaks at $\alpha\simeq\pi/6$ (modulo $\pm\pi$) changing into peaks at approximately $\pi/3$ intervals for larger $\tilde{R}$ values.

those for which one of the three DH wall orientations would provide null scattering in this triangular arrangement, as can be easily checked. The low efficiency in removing carriers away from these angles is therefore reflected in the peaks. This structure, however, only dominates at large $\tilde{R}$ values due to the large acceptance angle of scattering for small widths (see Figs. 3 and 4). This would provide a rather small scattering probability for a larger range of angles, which would then dilute the geometrical effect seen at larger $\tilde{R}$.

One might expect that this peculiar angular distribution could yield anomalously low resistivity values. However, we find that the values of $L\rho_{\Delta}$ are only slightly smaller ($\simeq 10\%$) than $L\rho_{\text{random}}$ for the same wall thickness and other parameters. For example, in the case of KC_{24} for $R=10\,\text{Å}$, $L\rho_{\text{random}}=1.50$ (see Table I), while $L\rho_{\Delta}=1.38(\times 10^{-11}\ \Omega\,\text{cm}^2)$. In fact, the dependence of ρ_{Δ} on R has the same general character as that shown in Fig. 5 for ρ_{random}. We therefore expect that it would be rather difficult to observe any difference between the resistivity values in the cases of a random- or a triangular-wall distribution. We speculate, however, that possible in-plane anisotropies in the resistivity would be detected in very sensitive and careful measurements done in restacking compounds.

V. DISCUSSION

We have presented a theoretical analysis of the very interesting electronic properties of DH domain walls.

The peculiar scattering properties of electrons in the graphitic conical bands have observable consequences, worthy of careful experimental investigation. Systematic residual resistivity measurements, like those currently being carried out,[16] together with microscopic observations of domain structure should provide a very sensitive test of the theoretical predictions.

The large residual resistivity values obtained for typical domain and wall sizes in the case of a random distribution of domains suggest that one may be able to set up a new macroscopic probe of the DH structure. These simpler measurements would complement microscopic techniques and could be used in the rapid characterization of sample structure. Also, the large sensitivity to the domain-wall width might prove useful in the study of the kinetics of intercalation.[7,15] This effect should contribute as well to the observed variation of the resistivity with pressure.[1,32]

On the other hand, the possibility of achieving vanishingly small residual resistance for an array of elongated domains with parallel walls is very appealing (as well as an in-plane anisotropy in the resistivity). This of course would be a direct test of the unusual scattering properties of the conduction carriers in these systems. There is also the added practical convenience of greatly reducing the residual resistivity in a sample by the careful manufacture of this special domain arrangement. The latter can be achieved in principle by the variation of the growing conditions, as suggested in some Monte Carlo simulations.[7]

The theory also predicts slightly lower residual resistivity values in the case of a "triangular" wall arrangement, in comparison with a random distribution. This special wall configuration would likely appear in the restacking guests and could also give rise to in-plane anisotropy in the residual resistivity. However, these effects are expected to be much more difficult to detect experimentally.

We have also presented an analysis of the inhomogeneous charge distribution across DH walls in a Thomas-Fermi approximation. The large charge depletion near the middle of the wall which produces carrier scattering would also affect the graphitic bond lengths in this region. These reduced bond-length changes could possibly reveal themselves in detailed diffraction measurements,[14] since one would expect that this effect would contribute to larger data dispersion in samples with a larger number of DH walls.

ACKNOWLEDGMENTS

We would like to thank D. Davidov for providing us with valuable experimental data prior to publication. This work was supported by the Natural Sciences and Engineering Research Council of Canada and by the Simon Fraser University President's Research Fund.

APPENDIX

Here we describe the procedure to obtain the tunneling coefficient $T(\theta)$ through a DH wall of width R which is characterized by the potential $V(x)$.

Because the potential varies only along the x direction, it is clear that the momentum in the y direction will be conserved during the scattering [see Eq. (2.6)], and that one can define

$$F_j(\mathbf{r})=g_j(x)e^{ik_y y}\ . \tag{A1}$$

The complex functions g_j satisfy two coupled one-dimensional equations,

$$\begin{aligned}[E-V(x)]g_1(x)&=-i\hbar v_F(k_y+d/dx)g_2(x)\ ,\\ [E-V(x)]g_2(x)&=-i\hbar v_F(d/dx-k_y)g_1(x)\ .\end{aligned} \tag{A2}$$

Since the potential V vanishes asymptotically on both sides of the wall, the solution to Eqs. (A2) in these regions can be constructed as linear combinations of functions similar to those in Eq. (2.11). For a particle incident *from the left* ($x\simeq-\infty$) with wave number k_x, the asymptotic wave functions g_j are the following:

$$\{g_1,g_2\}\cong A\{1,(k_x+ik_y)/k\}e^{ik_x x}+B\{1,(-k_x+ik_y)/k\}e^{-ik_x x}\quad \text{as } x\to-\infty \tag{A3}$$

and

$$\{g_1,g_2\}\cong\{1,(k_x+ik_y)/k\}e^{ik_x x}\quad \text{as } x\to+\infty\ , \tag{A4}$$

where $k=(k_x^2+k_y^2)^{1/2}$, and the complex constants A and B are uniquely determined below by solving Eqs. (A2). Notice that each term corresponds to traveling waves in each direction along the x axis and that the fluxes are normalized with respect to the outgoing flux at the far right ($x\simeq+\infty$). The tunneling and reflection coefficients are then given by $T=|A|^{-2}$ and $1-T=|B|^2/|A|^2$, respectively.

From Eq. (A3), we can obtain an expression for the magnitude of the constants A and B by decomposing all the terms in real and imaginary parts as

$$|A|^2=[(kg_{21}+k_xg_{11}+k_yg_{12})^2+(kg_{22}-k_yg_{11}+k_xg_{12})^2]/(4k_x^2) \quad \text{as } x\to-\infty \tag{A5}$$

and

$$|B|^2=[(kg_{21}-k_xg_{11}+k_yg_{12})^2+(kg_{22}-k_yg_{11}-k_xg_{12})^2]/(4k_x^2) \quad \text{as } x\to-\infty\ , \tag{A6}$$

where $g_j=g_{j1}+ig_{j2}$. In order to find the values of the g functions at the far left, and corresponding values for $|A|^2$ and $|B|^2$, we integrate Eqs. (A2) starting at the far right with Eqs. (A4). In these calculations we have operationally defined the asymptotic regions as those for which $V/\mu \leq 10^{-10}$ (see Sec. III). This procedure yields $T(k_x,k_y)$ which is plotted in Figs. 3 and 4 as function of the angle $\theta=\tan^{-1}(k_y/k_x)$, for constant k $(=k_F)$.

*Present address: Department of Physics and Astronomy, Ohio University, Athens, Ohio 45701.

[1]R. Clarke and C. Uher, Adv. Phys. **33**, 469 (1984).
[2]M. S. Dresselhaus and G. Dresselhaus, Adv. Phys. **30**, 139 (1981).
[3]S. E. Ulloa and G. Kirczenow, Comments Condensed Matter Phys. **12**, 181 (1986).
[4]N. Daumas and A. Hérold, C. R. Acad. Sci. Ser. C **268**, 373 (1969).
[5]A stage-m compound is an ordered sequence with a period of m host layers between adjacent intercalate layers.
[6]G. Forgács and G. Uimin, Phys. Rev. Lett. **52**, 633 (1984).
[7]G. Kirczenow, Phys. Rev. Lett. **55**, 2810 (1985); Synth. Met. **12**, 143 (1985).
[8]S. E. Ulloa and G. Kirczenow, Phys. Rev. Lett. **55**, 218 (1985); Phys. Rev. B **33**, 1360 (1986).
[9]D. T. Morelli and C. Uher, Phys. Rev. B **27**, 2477 (1983).
[10]M. S. Dresselhaus and G. Dresselhaus, Synth. Met. **12**, 79 (1985).
[11]D. P. DiVincenzo and E. J. Mele, Phys. Rev. B **29**, 1685 (1984).
[12]D. G. Onn, G. M. T. Foley, and J. E. Fischer, Phys. Rev. B **19**, 6474 (1979).
[13]L. Pietronero and S. Strassler, Phys. Rev. Lett. **47**, 593 (1981).
[14]W. A. Kamitakahara, J. L. Zarestky, and P. C. Eklund, Synth. Met. **12**, 301 (1985).
[15]I. Palchan, D. Davidov, V. Zenin, G. Polatsek, and H. Selig, Phys. Rev. B **32**, 5554 (1985).
[16]D. Vaknin, D. Davidov, and H. Selig (unpublished); I. Palchan, D. Vaknin, D. Davidov, and H. Selig (unpublished).
[17]A preliminary report has already been published, S. E. Ulloa and G. Kirczenow, Phys. Rev. Lett. **56**, 2537 (1986).
[18]J. Blinowski, H. H. Nguyen, C. Rigaux, J. P. Vieren, R. Le Toullec, G. Furdin, A. Hérold, and J. Melin, J. Phys. Paris **41**, 47 (1980).
[19]D. Hoffman, R. E. Heinz, G. L. Doll, and P. C. Eklund, Phys. Rev. B **32**, 1278 (1985).
[20]R. S. Markiewicz, Solid State Commun. **44**, 791 (1982).
[21]J. M. Luttinger and W. Kohn, Phys. Rev. **97**, 869 (1955); S. T. Pantelides, Rev. Mod. Phys. **50**, 797 (1978).
[22]J. C. Slonczewski and P. R. Weiss, Phys. Rev. **109**, 272 (1958).
[23]We remark that a very high degree of smoothness of the potential is not necessarily required. For example, we expect that, in the spirit of the effective-mass theory of shallow impurity states in semiconductors, the potential of a screened point charge may well be smooth enough to satisfy the present requirements (see Ref. 21).
[24]L. I. Schiff, *Quantum Mechanics*, 3rd ed. (McGraw-Hill, New York, 1968), p. 100.
[25](a) L. Pietronero, S. Strassler, H. R. Zeller, and M. J. Rice, Phys. Rev. Lett. **41**, 763 (1978); (b) Solid State Commun. **30**, 399 (1979).
[26]S. A. Safran and D. R. Hamann, Phys. Rev. B **22**, 606 (1980).
[27]Notice that for stages 1 and 2 which are considered here, all of the graphite layers are equivalent. In the case of higher stages, the formulation should include unequal layer occupation [see Ref. 25(b)]. Matching domain walls may possibly appear in stage-1 compounds where the intercalation is not complete or where some deintercalation has occurred.
[28]G. Campagnoli and E. Tosatti, J. Phys. C **15**, 1457 (1980).
[29]In writing Eqs. (3.1) and (3.2) we have ignored the effects of the elastic layer distortions which characterize the local wall configuration (see Ref. 8). The deformation potentials associated with this distortion should have much less influence on the local band structure than the Coulomb interactions considered here. Therefore, the main effect of the distortions would be geometrical in nature, effectively increasing the wall width by $<20\%$, even for staggered walls.
[30]R. E. Peierls, *Quantum Theory of Solids* (Oxford University Press, Oxford, 1955).
[31]In the case of stages 3 or higher, and in the stage 2 for very large DH wall widths (comparable to the intercalate domain size), one should consider percolation effects in treating the scattering problem by staging dislocations. In those instances, the average intercalate domain separation is comparable to the domain size, and the probability of electron-localization within a domain is large. An extreme limit would be reached whenever the resistivity *per layer* ρ becomes comparable to $1/\sigma_0\simeq 10^4\ \Omega/\square$, where $\sigma_0\simeq e^2/\hbar$ is the minimum metallic conductivity in a two-dimensional system [P.A. Lee and T. V. Ramakrishnan, Rev. Mod. Phys. **57**, 287 (1985)]. In the systems described in this paper, that limit would only be reached for very small values of the domain size, $L\simeq 10$ Å (see Fig. 5). Therefore, these localization effects should be not important in our discussion, since the most commonly observed domain sizes are much larger than the limits mentioned above. Notice also that we have neglected interlayer scattering since the corresponding matrix element is expected to be even smaller than in pristine graphite due to the larger carbon layer separation in the DH wall region.
[32]Y. Iye, O. Takahashi, S. Tanuma, K. Tsuji, and S. Minomura, J. Phys. Soc. Jpn. **51**, 475 (1982).
[33]T. C. Wu, F. L. Vogel, L. A. Pendrys, and C. Zeller, Mater. Sci. Eng. **47**, 161 (1981).
[34]C. Zeller, L. A. Pendrys, and F. L. Vogel, J. Mater. Sci. **14**, 2241 (1979).
[35]D. M. Hwang, X. W. Qian, and S. A. Solin, Phys. Rev. Lett. **53**, 1473 (1984); R. Levi-Setti, G. Crow, Y. L. Wang, N. W. Parker, R. Mittleman, and D. M. Hwang, *ibid.* **54**, 2615 (1985).
[36]M. E. Misenheimer and H. Zabel, Phys. Rev. Lett. **54**, 2521 (1985).